Journal of Materials Chemistry C

ROYAL SOCIETY OF CHEMISTRY

PAPER

View Article Online
View Journal | View Issue

Cite this: J. Mater. Chem. C, 2022, 10, 10742

Synthesis of asymmetric indolonaphthyridines with enhanced excited state charge-transfer character†

Michael Purdy, [a] Kealan Fallon, [a] Daniel G Congrave,[a] Daniel T. W. Toolan, [b] Weixuan Zeng [a] and Hugo Bronstein *[a]

Received 20th December 2021,
Accepted 20th May 2022

DOI: 10.1039/d1tc06054f

rsc.li/materials-c

Indolonaphthyridines (IND) are valuable chromophores with wide-ranging optoelectronic applications. Here, we present a new class of asymmetric IND derivatives, synthesised using novel high yielding methodology. We compare the absorption properties and excited state charge-transfer character of the novel assymetric INDs with symmetric IND. We show IND assymetry increases the change in dipole moment from ground to excited state. By determining the magnitude of the excited state dipole moment of each IND derivative, we also show assymetry increases excited state charge-transfer character. Quantum calculations indicate this is a consequence of increased spatial separation between excited state electron and hole wavefunctions for the assymetric INDs. Charge-transfer features can significantly benefit many optoelectronic processes, therefore the structure-property relationships introduced in this work provide invaluable design principles for the generation of high performance materials.

Introduction

Organic semiconductors (OSCs) are highly attractive materials for optoelectronic applications due to their light weight, low temperature processing, low production costs and above all tuneability.[1–3] The structure of OSCs can be tailored by chemists to create bespoke optoelectronic properties for high performance device application such as: organic light emitting diodes (OLEDs), organic solar cells (OSCs), organic field effect transistors (OFETs) and dye sensitised solar cells (DSCs).[4–7]

Molecular desymmetrisation is one method that can be used to tune the optoelectronic properties of OSCs and has been widely investigated in a variety of systems. Asymmetric diketopyrrolopyrrole (DPP) polymers have shown enhanced solubility and superb performance in OFET and OSC devices.[8–14] Ji *et al.* reported a series of DPP polymers with translational asymmetry along the conjugated backbone due to different thienyl substituents flanking the DPP core. The polymers exhibited high device performance due to significant thin-film crystallinity and were solution processed using non-polar solvents.[13] Wang *et al.* considerably enhanced the FET hole mobility of a DPP polymer by inducing alkyl chain asymmetry. By replacing one of the two branched alkyl chains on the DPP core with a linear chain, the interchain packing order and thin-film crystallinity were significantly improved.[8] Asymmetric arene diimides have also shown fascinating optoelectronic properties and excellent device performance.[15–17]

Asymmetry can enhance the excited state charge-transfer character of chromophores, wherein increased separation between electron and hole wavefunctions occurs after photoexcitation. Charge-transfer states have been shown to improve the performance of many optoelectronic applications. Charge-transfer states can increase the rate of singlet fission by mediating electronic coupling to a spin correlated triplet pair state involved in the mechanism. Charge-transfer states can also improve charge generation in organic solar cells and dye-sensitized solar cells by facilitating charge seperation.[18–20]

Indolonaphthyridine (IND), a bay-annulated indigo derivative, is a highly versatile chromophore for organic electronic applications. IND polymers and small molecules have been utilised in high-performance OFETs, OSCs, photodetectors and for photoacoustic imaging.[21–27] More recently, functionalised IND small molecules have been shown to undergo singlet fission, an exciton multiplication process that could be used to overcome the *Shockley–Queisser* limit placed on solar cells.[28]

Indolonaphthyridine thiophene (INDT) consists of an electron deficient IND core flanked by two thiophene (T) groups and is synthesised *via* an indigo double bay-annulation

[a] Department of Chemistry, University of Cambridge, Cambridge, CB2 1EW, UK. E-mail: hab60@cam.ac.uk
[b] Department of Chemistry, The University of Sheffield, Sheffield, S3 7HF, UK

† Electronic supplementary information (ESI) available. See DOI: https://doi.org/10.1039/d1tc06054f

reaction.[25] The planar aromatic core of INDT enables strong π–π stacking interactions which facilitates efficient charge transport but can also lead to poor solubility.[21] To address this, solubilising alkyl chains can be incorporated onto the IND core or thiophene groups, both of which suppress interchromophore interactions and enable solution processability.[21,23,24] The energy levels of INDT small molecules can be tuned *via* functionalisation of the indigo core. The thiophene groups can also act as a conjugating pathway to generate narrow band-gap polymers.[27,28]

Kolaczkowski *et al.* first reported desymmetrised INDT structures which were synthesised *via* step-wise bay annulation of indigo using different aromatic acetyl chlorides.[29] Here, asymmetry originated from the INDT core being flanked by different aryl groups, one thiophene and one phenyl, which enabled selective monobromination and synthesis of larger donor–acceptor constructs. However, the reliance on a condensation reaction using aromatic acetyl chlorides as the only method of indigo bay annulation resulted in asymmetric structures that were limited to only phenyl and thienyl groups. Here, we offer a new innovative methodology to generate desymmetrised IND structures that have only one aromatic group flanking the core. We introduce novel indigo bay annulation reactions that are facile and high yielding. As the novel chromophore contains only half the solubilising groups of a symmetric IND, we also develop a novel synthesis of an alkylated indigo, which ensures heightened control over the materials solubility. Notably, the removal of a flanking aromatic unit leads to a wider band gap material with blue shifted absorption characteristics, thus fine tuning the excited state energy levels for singlet fission solar cell applications. Furthermore, we use absorption and emission spectroscopy, in conjunction with quantum calculations, to show desymmetisation leads to enhanced excited state charge-transfer character of INDTs. As stated previously, charge transfer states can improve the performance of many optoelectronic processes. Therefore the enhanced excited state charge transfer character of the asymmetric IND derivatives could potentially generate exceptionally high-performance materials.

Synthesis

5,5′-Dihexylindigo synthesis

Alkyl chains can be incorporated into chromophores to ensure high solubility by supressing π–π stacking interactions. For this reason, 5,5′-dihexylindigo **5** is synthesised as the indigo substrate for the subsequent annulation reactions. The procedure for 5,5′-dihexylindigo synthesis is inspired from the traditional isatin self-condensation route for indigo synthesis (Scheme 1(a)). *O*-Benzylhydroxyl amine **1**, is converted to **2** *via* imine condensation with glyoxylic acid. Iminoacetic acid **2** is subsequently converted to an acid chloride which undergoes nucleophilic attack by 4-hexylaniline to give acetamide **3** which is then subjected to acid catalysed imine hydrolysis with ring-closure, yielding hexylated isatin **4**. In the presence of phosphorous pentachloride and thiophenol, **4** undergoes self-condensation to produce alkylated indigo **5**.

INDT synthesis

Symmetrical IND (**S-INDT**) is synthesised *via* a bay annulation condensation reaction of **5** with 2-(5-(2-ethylhexyl)thiophen-2-yl)acetyl chloride in 4% yield. The reaction requires refluxing at high temperatures overnight whilst exposed to air and the condensation step produces water as a by-product which can destroy the acid chloride. This results in a vast number of by-products being produced and extensive purification (2× chromatography on silica gel, trituration and recrystallization) is required to obtain pure product. Synthesis of the asymmetric INDs involves initially converting **5** to half-annulated indigoid **7** (Scheme 1(b)) by adapting a procedure developed by Kuzmich *et al.*[30] **5** is deprotonated using sodium hydride and then reacted with diethyl malonate. The reaction work-up is facile; the product is precipitated in weakly acidic solution, washed with small amounts of MeOH and air-dried leaving pure material. The reaction time is significantly shorter (45 min) and the yield (82%) is exceptionally high for a selective indigo mono-bay annulation reaction. **8** then undergoes an annulation reaction with 2-(5-(2-ethylhexyl)thiophen-2-yl)acetyl chloride, producing **AE-INDT** (**8**) in 35% yield. The reaction conditions are the same as **S-INDT** synthesis however the yields are considerably higher. The number of by-products were significantly reduced in the **AE-INDT** synthesis relative to **S-INDT** which indicates the rate of product formation relatively outcompetes by-product formation. This could be attributed to a number of factors: the formation of **8** requires only one annulation whereas **6** requires two; the solubility of asymmetric indigoid **7** is considerably higher than **5**; the presence of an electron deficient ester group activates **7** and encourages bond formation with an electron rich thienyl group. Finally, decarboxylation of **8** *via* heating in hydrobromic acid afforded **AH-INDT** (**9**) in 80% yield. The purification of **9** involved only aqueous work-up and trituration, again showcasing how this novel methodology boasts shorter reaction times, higher yields and straightforward purification.

Results and discussion

Optical properties

Molecular symmetry often plays an extremely important role in the optical properties of conjugated materials; however it has scarcely been investigated in popular optoelectronic systems. Therefore, it is important to fully investigate the effects of structural desymmetrisation on the fundamental properties of these molecules. This sheds light, not only on new materials but allows detailed structure-property relationship to be developed for both symmetric and asymmetric derivates.

All three materials showed strong absorption in the red region of the visible spectrum (Fig. 1). The optical band gaps of **S-INDT**, **AE-INDT** and **AH-INDT** are estimated from the onset of the solution state absorption spectrum presented in Fig. 1,

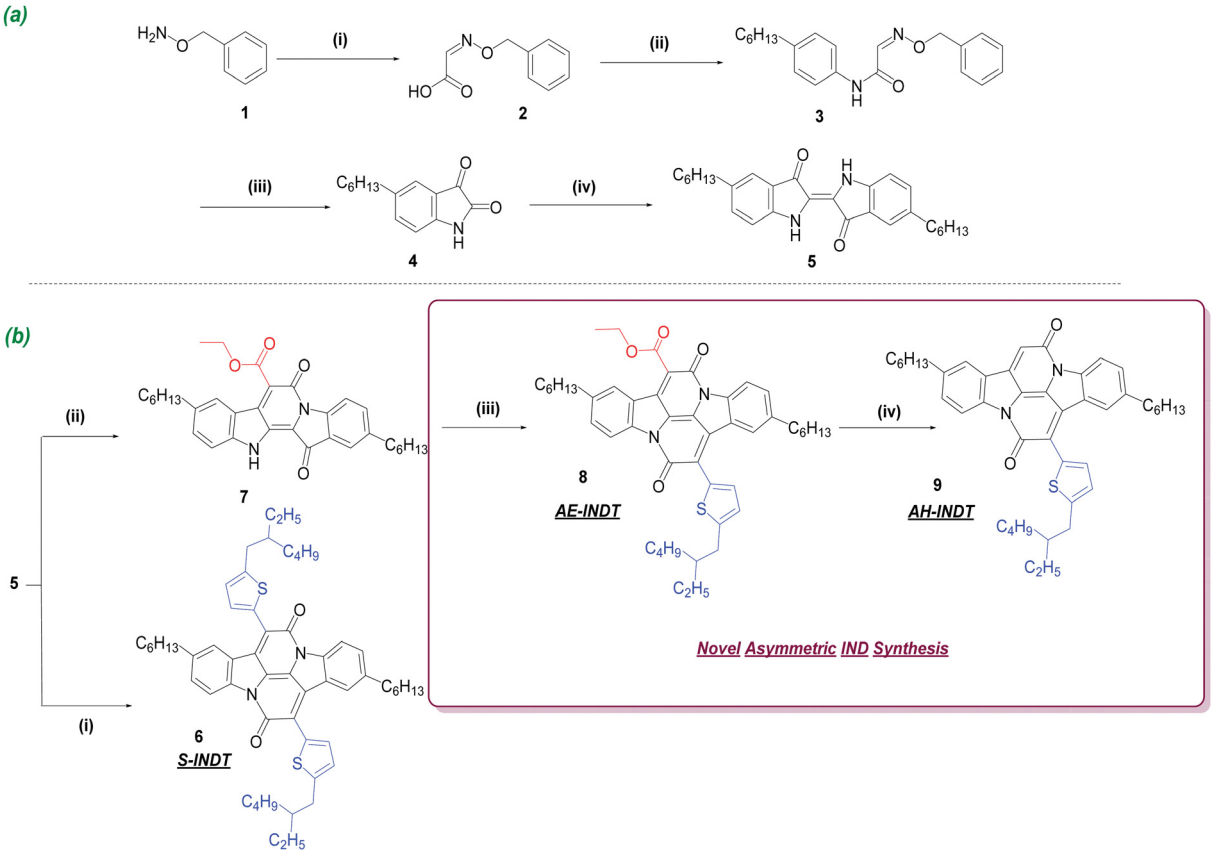

Scheme 1 (a) Synthesis 5,5′-dihexylindigo. *Reagents and conditions*: (i) glyoxylic acid (2 equiv.), H_2O, r.t., 2 h (93%). (ii) 1. Thionyl chloride (3 equiv.), *N*,*N*-dimethylformamide (DMF) (1 drop), dichloromethane (DCM), reflux, 3 h. 2. 4-Hexylanaline (1 equiv.), *N*,*N*-Diisopropylethylamine (DIPEA) (1.2 equiv.), DCM, r.t., 12 h (82%). (iii) H_2SO_4 (3 mL g^{-1}), 50 → 80 °C, 1.1 h (89%). (iv) Phosphorus pentachloride (1.1 equiv.), thiophenol (2.3 equiv.), 100 → 50 °C, 16 h (30%). (b) Synthesis of INDT Derivatives. *Reagents and conditions*: (i) acid chloride (8 equiv.), xylenes, reflux, 12 h, (4%). (ii) Sodium hydride (6 equiv.), diethyl malonate (4 equiv.), DMF, reflux, 0.5 h (80%). (iii) Acid chloride (6 equiv.), xylenes, reflux, 12 h (35%). (iv) 47% HBr 0.2 mL g^{-1} (substrate), reflux, 2 h (75%).

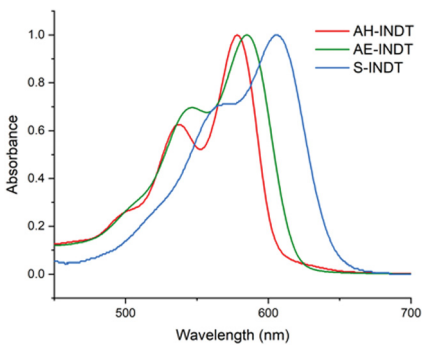

Fig. 1 UV-Vis absorption spectra of IND derivatives in hexane solution.

and are found to be 1.91 eV, 2.00 eV and 2.05 eV respectively. Reduced conjugation length throughout the IND core therefore increases the optical band-gap. Time-dependent density functional theory (TD-DFT) calculations of optimised structures presented in Table S1, ESI† reflect this trend. The extinction co-efficients of **S-INDT**, **AE-INDT** and **AH-INDT** are 13 000, 6700 and 7100 M^{-1} cm^{-1} respectively. The photoluminescent quantum yields in solution of **S-INDT**, **AE-INDT** and **AH-INDT** are 62%, 23% and 22%. These optical measurements show the asymmetric IND derivatives have reduced absorption and photoluminescence strength relative to **S-INDT**. This was verified computationally, where the oscillator strengths of the S_1 transition were estimated from TD-DFT calculations and found to be larger for **S-INDT** (0.75) relative to **AE-INDT** (0.54) and **AH-INDT** (0.47). Interestingly, the HOMO–LUMO overlap integral was calculated to be approximately the same for each INDT derivative. The reduced oscillator strength of the **AE-INDT** and **AH-INDT** S_1 transition is therefore likely a consequence of other complex factors that affect the transition dipole moment and not a result of reduced frontier molecular overlap (*i.e.* direct CT character).

Charge-transfer character

The optical properties of INDs (and related chromophores – *e.g.* DPP, IsoIndigo, Indigo) are often attributed to charge transfer like absorptions due to the presence of both electron rich and poor substituents. Therefore we hypothesized that introducing asymmetry into this system could have an effect on the extent of charge-transfer in the optical transitions. This was investigated by testing the compounds for solvatochromism.

The solution state absorption and photoluminescence were measured in a range of solvents of different polarities (Fig. 2).

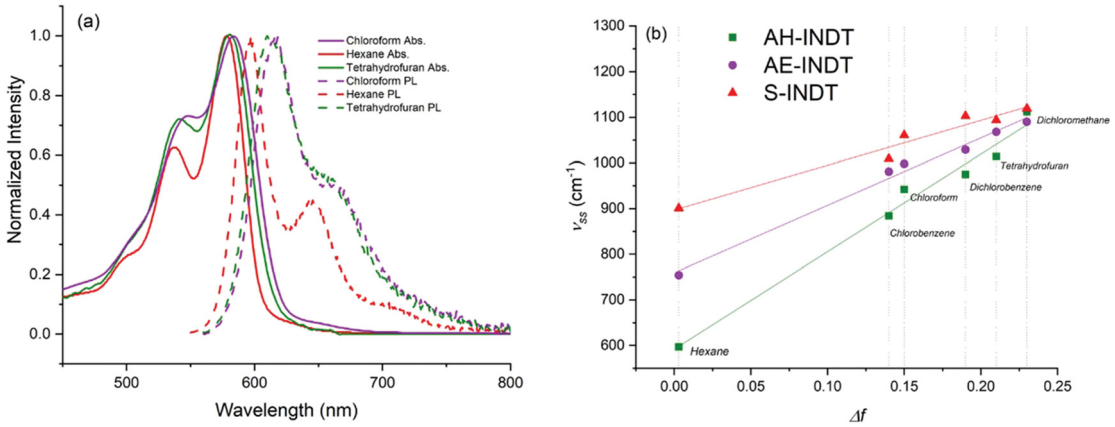

Fig. 2 (a) Absorbance and emission spectra of and AH-INDT in solvents of different polarity. The measurements were performed in 6 different solvents however only 3 have been included for clarity. (b) Lippert-Mataga plot of each IND derivative showing all 6 solvents.

In general, we observed that the symmetrical derivative displayed very little solvatochromic behaviour, whereas the two new asymmetric materials showed a range of behaviour on increasing solvent polarity.

We investigated the differences in dipole moment change from ground to excited state ($\Delta\mu_{ge}$) using the Lippert–Mataga equation, wherein the Stokes shift (ν_{ss}) of each derivative in different solvents is plotted against solvent orientation polarizability (Δf).[31]

The change in dipole moment ($\Delta\mu_{ge}$) is estimated from the gradient of a Lippert–Mataga plot (Fig. 2). All three INDT derivatives showed increasing ν_{ss} with Δf however at different rates of change. **S-INDT** had the lowest rate of change and a value of 4.67 *D* was determined for $\Delta\mu_{ge}$. **AE-INDT** Stokes shift also gradually increases with increasing Δf but at a higher rate than **S-INDT** and a value of 5.74 *D* was determined for $\Delta\mu_{ge}$. **AH-INDT** has the highest rate of Stokes shift increase with increasing Δf and a value of 6.91 *D* is determined for $\Delta\mu_{ge}$.

DFT calculations were used to estimate the ground state dipole moment (μ_g). **S-INDT** was predicted to have the lowest μ_g (0.19 *D*) due to increased molecular symmetry. **AE-INDT** was predicted to have a higher μ_g than **AH-INDT**, with 2.69 *D* and 1.48 *D* respectively. This is likely due to the presence of an electron withdrawing ester group extended from the core of **AE-INDT** which would create a more electronically polarised ground state.

The excited state dipole moment (μ_e) of each IND derivative was determined using the experimentally determined $\Delta\mu_{ge}$ and μ_g estimated from DFT. **S-INDT** was found to have the lowest value of 4.8 *D*. **AE-INDT** and **AH-INDT** were determined to have approximately the same μ_e with 8.43 *D* and 8. 39 *D* respectively. Thus **AE-INDT** and **AH-INDT** have larger excited state dipole moments relative to **S-INDT** and therefore have increased charge-transfer state contribution to the excited state.

The excited state charge transfer length (*D*) is the predicted distance between the centroid of the electron and hole in the excited state and was estimated to be lower for **S-INDT** (0.08 Å) relative to **AE-INDT** (0.74 Å) and **AH-INDT** (0.76 Å) in the S_1 state. The Sr index estimates the overlap of the electron and hole wavefunction and was estimated to be the same for each INDT derivative (Table 1). The larger μ_e determined for **AE-INDT** and **AH-INDT** relative to **S-INDT** is therefore likely due to increased spatial separation between the centre of charges in the S_1 state.

IND desymmetrisation and solid-state interactions

Desymmetrisation can significantly affect solid-state interactions which are highly influential to all other aforementioned optoelectronic applications. Therefore we performed absorption spectroscopy on thin-films of each IND derivative to

Table 1 Optical properties of IND series

Molecule	Optical band gap[a] (eV)	S_1 state energy[b] (eV)	Oscillator strength of S_1 transition[c]	HOMO–LUMO overlap integral[d]	Extinction coefficient[e] (1×10^4 M^{-1} cm^{-1})	μ_g[f] (D)	$\Delta\mu_{ge}$ of S_1 state excitation[g] (D)	μ_e of S_1 state[h] (D)	*D* index (Å) S_1 state[i]	Sr index (a.u.) S_1 state[j]	PLQY[k] (%)
S-INDT	1.91	2.42	0.75	0.80	1.30	0.19	4.67	4.86	0.08	0.76	62
AE-INDT	2.00	2.51	0.54	0.80	0.67	2.69	5.74	8.43	0.74	0.76	23
AH-INDT	2.05	2.62	0.47	0.79	0.71	1.48	6.91	8.39	0.76	0.76	22

[a] Optical band gaps estimated from on-set of UV-Vis absorption spectra. [b] Energies of the first singlet (S_1) excited states. [c] Estimated oscillator strength of S_1 transition from multiwfn calculation. [d] Estimated HOMO–LUMO overlap integral from multiwfn calculation. [e] Extinction coefficient extrapolated from change in UV-Vis absorption intensity with sample concentration. [f] Ground state dipole moment taken from DFT optimised structures. [g] Change in dipole moment extrapolated from Lippert–Mataga plot. [h] Excited state dipole moment calculation from *a* and *b*. [i] The excited state charge-transfer length calculated using multiwfn. [j] The overlap of the electron and hole wavefunction calculated using multiwfn. [k] PLQY measurements performed in tetrahydrofuran solution.

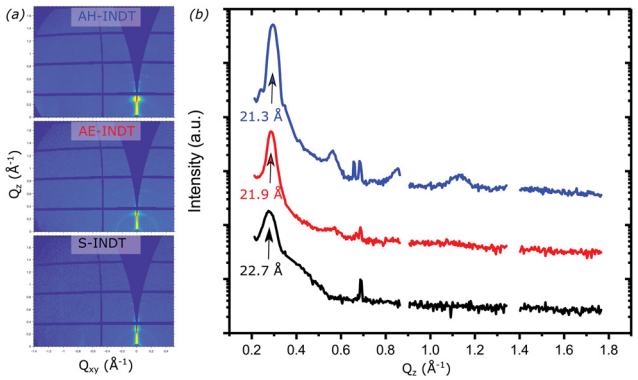

Fig. 3 (a) Two-dimension grazing incidence scattering data for S-INDT (bottom), AE-INDT (middle) and AH-INDT (top) and (b) corresponding in-plane linecuts for S-INDT (black), AE-INDT (red) and AH-INDT (blue).

investigate the effect of IND desymmetrisation on solid-state interactions.

The structure of the thin-film absorption spectra relative to solution-state is considerably altered for **AE-INDT** and **AH-INDT** relative to **S-INDT** (see ESI†). This indicates IND asymmetry results in considerably different solid state interactions. **AE-INDT** and **AH-INDT** both exhibit predominantly H-like aggregation in the solid state, wherein the solid-state absorption maximum is hypsochromically shifted relative to the solution-state absorption maximum. **S-INDT** however exhibits solid-state J-like aggregation, wherein the solid-state absorption maximum is bathochromically shifted relative to the solution-state absorption maximum. Grazing incidence wide-angle X-ray scattering (GIWAXS) was employed to gain further insight into microstructure of the IND films (Fig. 3). All films exhibit a strong in-plane scattering feature $Q_z \sim 0.29$ Å^{-1}, with a weaker Debye–Scherrer ring at this lengthscale. This is consistent with the IND films forming a lamella packed structure with a pronounced in-plane orientation.[25] For the IND series the introduction of asymmetry results in an increase in the magnitude of this scattering feature, indicative of greater film crystallinity. In addition to the lamella scattering feature at higher $Q \sim 0.68$ Å^{-1} additional sharp crystalline peaks are observed, most likely arising due to the crystallization of the alkyl side chains of the IND. The scattering data show that the introduction of IND asymmetry results in greater thin-film crystallinity and a slight reduction in the lamella spacing from 22.7 Å (**S-INDT**) to 21.3 (**AH-INDT**).

The observed differences in solid-state behaviour could have a profound impact on IND singlet fission rate. Singlet fission is highly dependent on the extent of electronic coupling between monomers in the solid-state.[32] Therefore, the stronger solid-state π–π interactions could increase the rate of singlet fission for the asymmetric INDs relative **S-INDT**. The study by Fallon *et al.* showed all functionalised IND small molecules that exhibited singlet fission also showed H-aggregation in the solid-state.[28] As the asymmetric INDs exhibit H-aggregation whereas **S-INDT** exhibits J-aggregation, this further indicates desymmetrisation creates more favourable solid-state interactions for singlet fission.

Conclusions

In conclusion, we have developed a series of novel asymmetric IND derivatives that exhibit increased excited state charge-transfer contribution relative to symmetrical IND. The novel indigo bay annulation reactions we introduce overcomes many of the issues associated with traditional indigo condensation bay annulation reactions, particularly low reaction yields and protracted purification. Our in-depth analysis of the relationship between symmetry and solvatochromism in INDs furthers our understanding of excited state intramolecular charge transfer in these systems. We show how desymmetrisation increases the distance between the centroid of the electron and hole after photoexcitation and therefore increases excited state charge transfer character. The increased solvatochromism observed in **AH-INDT** relative to **AE-INDT** also shows the magnitude of the ground state dipole moment does not pre-determine solvatochromic sensitivity after photoexcitation. Through extinction co-efficient measurements, we show asymmetry reduces the absorption strength of INDTs and that excited state charge transfer directly affects the optoelectronic properties of these materials. The asymmetric INDs also show enhanced π–π interactions and H-aggregation in the solid-state. This indicates desymmetrisation may favour increased rates of singlet fission.

Computational method

Quantum calculations were performed on each structure to investigate the differences in excited state energies, ground state dipole moment and excited state charge-transfer length for all molecules introduced in this work. All S_0 optimized geometries were obtained using the B3LYP functional together with the 6-311G** basis set.[28,33] Based on the optimized ground state geometries, the ground state dipole moments were determined and the vertical excitation energy levels were evaluated at TD-DFT M06-2X/6-311G** level.[28] The S_1 state charge-transfer lengths were analysed with Multiwfn 3.7.[34]

Author contributions

The manuscript was completed through contribution from all authors.

Conflicts of interest

There are no conflicts to declare.

Acknowledgements

This work was supported by the Engineering and Physical Sciences Research Council (EP/S003126/1).

References

1 V. Coropceanu, H. Li, P. Winget, L. Zhu and J. L. Brédas, *Annu. Rev. Mater. Res.*, 2013, **43**, 63–87.
2 V. Coropceanu, J. Cornil, D. A. da Silva Filho, Y. Olivier, R. Silbey and J. L. Brédas, *Chem. Rev.*, 2007, **107**, 926–952.
3 A. Rahmanudin, R. Marcial-Hernandez, A. Zamhuri, A. S. Walton, D. J. Tate, R. U. Khan, S. Aphichatpanichakul, A. B. Foster, S. Broll and M. L. Turner, *Adv. Sci.*, 2020, **7**, 2002010.
4 S. Liu, J. Yuan, W. Deng, M. Luo, Y. Xie, Q. Liang, Y. Zou, Z. He, H. Wu and Y. Cao, *Nat. Photonics*, 2020, **14**, 300–305.
5 R. Y. Ogura, S. Nakane, M. Morooka, M. Orihashi, Y. Suzuki and K. Noda, *Appl. Phys. Lett.*, 2009, **94**, 073308.
6 Q. Wang, S. Jiang, J. Qian, L. Song, L. Zhang, Y. Zhang, Y. Zhang, Y. Wang, X. Wang, Y. Shi, Y. Zheng and Y. Li, *Sci. Rep.*, 2017, **7**, 7830.
7 T. Matsushima, F. Bencheikh, T. Komino, M. R. Leyden, A. S.-D. Sandanayaka, C. Qin and C. Adachi, *Nature*, 2019, **572**, 502–506.
8 Z. Wang, Z. Liu, L. Ning, M. Xiao, Y. Yi, Z. Cai, A. Sadhanala, G. Zhang, W. Chen, H. Sirringhaus and D. Zhang, *Chem. Mater.*, 2018, **30**, 3090–3100.
9 B. Metten, K. Martinez, J. Thomas, W. Qin, M. Smet, N. Boens and W. Dehaen, *Org. Biomol. Chem.*, 2007, **5**, 2587–2591.
10 J. Ji, X. Wu, P. Deng, D. Zhou, D. Lai, H. Zhan and H. Chen, *J. Mater. Chem. C*, 2019, **7**, 10860–10867.
11 Z. Jiang, Z. Ni, H. Wang, Z. Wang, J. Zhang, G. Qiu, J. Fang, Y. Zhang, H. Dong, K. Lu, W. Hu and Z. Wei, *Polym. Chem.*, 2017, **8**, 5603–5610.
12 P. J. Leenaers, M. M. Wienk and R. A.-J. Janssen, *Org. Electron.*, 2020, **86**, 105914.
13 Y. Ji, C. Xiao, Q. Wang, J. Zhang, C. Li, Y. Wu, Z. Wei, X. Zhan, W. Hu, Z. Wang, R. A.-J. Janssen and W. Li, *Adv. Mater.*, 2016, **28**, 943–950.
14 L. Sharma and H. Bronstein, *RSC Adv.*, 2021, **11**, 5276–5283.
15 W. Chen, J. Zhang, G. Long, Y. Liu and Q. Zhang, *J. Mater. Chem. C*, 2015, **3**, 8219–8224.
16 K. Tambara, N. Ponnuswamy, G. Hennrich and G. D. Pantoş, *J. Org. Chem.*, 2011, **76**, 3338–3347.
17 Y. Che, A. Datar, K. Balakrishnan and L. Zang, *J. Am. Chem. Soc.*, 2007, **129**, 7234–7235.
18 J. C. Brauer, A. Marchioro, A. A. Paraecattil, A. A. Oskouei and J. E. Moser, *J. Phys. Chem. C*, 2015, **119**, 26266–26274.
19 V. Coropceanu, X. K. Chen, T. Wang, Z. Zheng and J. L. Brédas, *Nat. Rev. Mater.*, 2019, **4**, 689–707.
20 N. Monahan and X. Y. Zhu, *Annu. Rev. Phys. Chem.*, 2015, **66**, 601–618.
21 B. He, A. B. Pun, D. Zherebetskyy, Y. Liu, F. Liu, L. M. Klivansky, A. M. McGough, B. A. Zhang, K. Lo, T. P. Russell, L. Wang and Y. Liu, *J. Am. Chem. Soc.*, 2014, **136**, 15093–15101.
22 M. A. Kolaczkowski and Y. Liu, *Chem. Rec.*, 2019, **19**, 1062–1077.
23 K. J. Fallon, A. Santala, N. Wijeyasinghe, E. F. Manley, N. Goodeal, A. Leventis, D. M.-E. Freeman, M. Al-Hashimi, L. X. Chen, T. J. Marks, T. D. Anthopoulos and H. Bronstein, *Adv. Funct. Mater.*, 2017, **27**, 1704069.
24 F. Verstraeten, S. Gielen, P. Verstappen, J. Kesters, E. Georgitzikis, J. Raymakers, D. Cheyns, P. Malinowski, M. Daenen, L. Lutsen, K. Vandewal and W. Maes, *J. Mater. Chem. C*, 2018, **6**, 11645–11650.
25 K. J. Fallon, N. Wijeyasinghe, E. F. Manley, S. D. Dimitrov, S. A. Yousaf, R. S. Ashraf, W. Duffy, A. A.-Y. Guilbert, D. M.-E. Freeman, M. Al-Hashimi, J. Nelson, J. R. Durrant, L. X. Chen, I. McCulloch, T. J. Marks, T. M. Clarke, T. D. Anthopoulos and H. Bronstein, *Chem. Mater.*, 2016, **28**, 8366–8378.
26 K. J. Fallon and H. Bronstein, *Acc. Chem. Res.*, 2021, **54**, 182–193.
27 K. J. Fallon, N. Wijeyasinghe, N. Yaacobi-Gross, R. S. Ashraf, D. M.-E. Freeman, R. G. Palgrave, M. Al-Hashimi, T. J. Marks, I. McCulloch, T. D. Anthopoulos and H. Bronstein, *Macromolecules*, 2015, **48**, 5148–5154.
28 K. J. Fallon, P. Budden, E. Salvadori, A. M. Ganose, C. N. Savory, L. Eyre, S. Dowland, Q. Ai, S. Goodlett, C. Risko, D. O. Scanlon, C. W.-M. Kay, A. Rao, R. H. Friend, A. J. Musser and H. Bronstein, *J. Am. Chem. Soc.*, 2019, **141**, 13867–13876.
29 M. A. Kolaczkowski, B. He and Y. Liu, *Org. Lett.*, 2016, **18**, 5224–5227.
30 M. E. Zhidkov, A. V. Kantemirov, A. V. Koisevnikov, A. N. Andin and A. S. Kuzmich, *Tetrahedron Lett.*, 2018, **59**, 708–711.
31 N. A. Sayresmith, A. Saminathan, J. K. Sailer, S. M. Patberg, K. Sandor, Y. Krishnan and M. G. Walter, *J. Am. Chem. Soc.*, 2019, **141**, 18780–18790.
32 R. D. Pensack, A. J. Tilley, C. Grieco, G. E. Purdum, E. E. Ostroumov, D. B. Granger, D. G. Oblinsky, J. C. Dean, G. S. Doucette, J. B. Asbury, Y. L. Loo, D. S. Seferos, J. E. Anthony and G. D. Scholes, *Chem. Sci.*, 2018, **9**, 6240–6259.
33 W. Zeng, O. El Bakouri, D. W. Szczepanik, H. Bronstein and H. Ottosson, *Chem. Sci.*, 2021, **12**, 6159–6171.
34 T. Lu and F. Chen, *J. Comput. Chem.*, 2012, **33**, 580–592.